Article:

Streets, A.J., Magayr, T.A., Huang, L. et al. (6 more authors) (2017) Parallel microarray profiling identifies ErbB4 as a determinant of cyst growth in ADPKD and a prognostic biomarker for disease progression. American Journal of Physiology - Renal Physiology, 312 (4). F577-F588. ISSN 1931-857X

https://doi.org/10.1152/ajprenal.00607.2016

Articles in PresS. Am J Physiol Renal Physiol (January 11, 2017). doi:10.1152/ajprenal.00607.2016

Parallel microarray profiling identifies ErbB4 as a determinant of cyst growth in ADPKD and a prognostic biomarker for disease progression

Andrew J Streets[1], Tajdida A Magayr[1], Linghong Huang[1], Laura Vergoz[1], Sandro Rossetti[2], Roslyn J Simms[1], Peter C Harris[2], Dorien JM Peters[3], Albert CM Ong[1]

[1]Kidney Genetics Group, Academic Unit of Nephrology, The Medical School, University of Sheffield, UK, [2]Division of Nephrology, Mayo Clinic and Foundation, Rochester, MN55905, USA, [3]Department of Human Genetics, Leiden University Medical Center, Leiden, The Netherlands

Running Head

ErbB4 expression and ADPKD disease progression

Correspondence:

AJ Streets (a.j.streets@sheffield.ac.uk)

Kidney Genetics Group, Academic Unit of Nephrology, The Medical School, University of Sheffield, Beech Hill Road, Sheffield S10 2RX, UK

Tel:+44 114 215 9555

Abstract

Autosomal Dominant Polycystic Kidney Disease (ADPKD) is the fourth most common cause of end-stage renal disease. The disease course can be highly variable and treatment options are limited. To identify new therapeutic targets and prognostic biomarkers of disease, we conducted parallel discovery microarray profiling in normal and diseased human *PKD1* cystic kidney cells. A total of 1515 genes and 5 miRNA were differentially expressed by more than two-fold in *PKD1* cells. Functional enrichment analysis identified 30 dysregulated signalling pathways including the epidermal growth factor (EGF) receptor pathway. In this paper, we report that the EGF/ErbB family receptor, ErbB4, is a major factor driving cyst growth in ADPKD. Expression of ErbB4 *in vivo* was increased in human ADPKD and *Pkd1* cystic kidneys, both transcriptionally and post-transcriptionally by mir-193b-3p. Ligand-induced activation of ErbB4 drives cystic proliferation and expansion suggesting a pathogenic role in cystogenesis. Our results implicate ErbB4 activation as functionally relevant in ADPKD, both as a marker of disease activity and as a new therapeutic target in this major kidney disease.

Keywords

ADPKD, ErbB4, microRNA, Polycystin

Introduction

Autosomal dominant polycystic kidney disease (ADPKD) is the most common genetic disease affecting the kidney (incidence 1 in 1,000) and is caused by mutations in two genes, *PKD1* (85-90%) or *PKD2* (10-15%) (21). Around 10% of patients requiring renal replacement therapy have ADPKD making it a major economic, medical and psychosocial burden worldwide (21). Recent studies have confirmed strong genic and allelic influences on the age of end-stage renal disease (ESRD) (4). However, the course of disease can be highly variable with evidence of intra-familial variability indicating the likely influence of other genetic factors (modifying genes, microRNAs), epigenetic factors and environmental triggers.

The recent approval of the vasopressin type 2 receptor antagonist, tolvaptan, for ADPKD patients with mild to moderate chronic kidney disease (eGFR >30ml/min/1.73m^2) and evidence of rapid disease progression represents a step-change in the management of this condition (8, 16). However, the drug is only moderately effective and has significant side-effects including a risk of liver toxicity, limiting its use and requiring frequent monitoring. There is therefore a need to develop more effective and safer drugs, which could also be used in combination. In addition, the identification of new prognostic biomarkers would be a major advance, especially in the early stages of disease, before significant increases in cystic burden occur (as measured by total kidney volume).

To identify new therapeutic targets and prognostic biomarkers in ADPKD, we conducted parallel microarray discovery profiling in normal and diseased human *PKD1* cystic kidney cells, generated from nephrectomy tissue. Our results identify 30 dysregulated signalling pathways when genes altered by at least 2-fold in abundance are analysed. Among these was the EGF receptor signalling pathway, several members of which have been previously implicated in PKD pathogenesis. In this paper, we report that expression and activation of the EGF-related receptor, ErbB4, is increased in human and mouse models and that this drives cyst proliferation and expansion in vitro. We also demonstrate that ErbB4 is a target for mir-193b-3p, a novel finding. Finally, we show that urine exosome ErbB4 correlates significantly with the rate of renal disease progression (eGFR slope), providing additional prognostic value to mean kidney length (measured by ultrasound) in ROC analysis. These results indicate that activation of the ErbB4 pathway is functionally relevant in ADPKD pathogenesis, reflects disease activity and represents a new potential therapeutic target in this disease.

Materials and Methods

Materials

All chemicals were purchased from Sigma Chemical (Poole, Dorset, United Kingdom), unless otherwise stated.

Cell Lines

Non-cystic (UCL93, RFH) and cystic (OX161, OX938, SKI-001, SKI-002) epithelial cells were immortalised from primary cultures of tubular cells isolated from normal and ADPKD human kidneys removed for clinical indications as previously described (24). SKI-002 cells were found to carry germline (IVS25-3C>G) and somatic (2312_2324del) *PKD1* mutations both of which are predicted to result in premature protein truncation.

Cells were grown in Dulbecco's Modified Eagles Medium-Ham's 12 (DMEM-F12, Invitrogen) supplemented with 1% L-Glutamine (Invitrogen), 5% NuSerum (Becton Dickinson) and 1% antibiotic/antimycotic solution (Invitrogen) at 33°C/5% CO_2. HEK-293 cells and control CL8 and CL11 kidney epithelial cells were cultured in Dulbecco's Modified Eagles Medium-Ham's 12 (DMEM-F12, Invitrogen) supplemented with 1% L-Glutamine (Invitrogen), 10% FCS and 1% antibiotic/antimycotic solution (Invitrogen) at 37°C/5% CO_2.

Transfections

Cells were transfected with a plasmid expressing the JM-A CYT-1 isoform of ErbB4 (Addgene plasmid #29527, pcDNA3.1-ErbB4) using Lipofectamine 2000 for 48h prior to the cell proliferation assays. In some experiments, cells were transfected with negative control or mir-193b-3p miRNA mimic (Life Technologies) using RNAiMax (Life Technologies).

RNA extraction and microarray

Total RNA was extracted from cells using Trizol according to the manufacturer's protocol (Life Technologies). All human cells were maintained and RNA extracted between passages 10-20. Prior to RNA extraction, cells were synchronised by serum starvation for 24h followed by reintroduction of serum for 24h in order to standardise the growth conditions between the different cell lines. RNA quality was determined using an Agilent 2100 BioAnalyser. Parallel mRNA and miRNA microarrays were carried out on Agilent human mRNA microarray (SurePrint G3 Human Gene Expression 8x60K v2 Microarray, one glass slide formatted with eight high-definition 60K arrays) or human miRNA microarray (Release 19.0, 8x60K, one glass slide formatted with eight high-definition 60K arrays based on miRBase Release 19.0) respectively.

A guided workflow based on Agilent single colour expression data within Agilent GeneSpring GX software was used to identify differentially expressed mRNA and miRNA. Briefly the guided workflow carries out a thresholding of the signal values to 5 followed by log transformation. It then normalizes the data to the 75th percentile and performs baseline transformation to the median of all samples. Samples are then divided into experimental groups and entities filtered based on their flag values: P(present), M(marginal) and A(absent). Only entities having the present and marginal flags in at least 1 sample are displayed. Differential expression significance analysis is performed by unpaired T-test and p-values >0.05 were defined as significant. Fold change analysis is then used to identify genes with expression ratios or differences between ADPKD and control cells that are outside of a given cutoff or threshold. Fold change gives the absolute ratio of normalized intensities (no log scale) between the average intensities of the samples grouped. The entities satisfying the significance analysis are passed on for the fold change analysis. All array files are available from the ABI ArrayExpress database (accession number(s) E-MTAB-4188, E-MTAB-4189)

Pathway analysis was carried out using The PANTHER (Protein ANalysis THrough Evolutionary Relationships) classification system which was designed to classify proteins (and their genes) in order to facilitate high-throughput analysis. All genes which showed a >2 fold change in expression in ADPKD cell lines were mapped to PANTHER pathways which consists of over 177 primarily signalling pathways. Pathways which were statistically overrepresented (p>0.05) were then identified.

Quantitative PCR

Relative ErbB4 and mir-193b-3p expression between control (n=4) and ADPKD (n=4) cells as well as in isolated exosomes purified from human urine samples was determined by Taqman qPCR according to the manufacturer's protocol (Life Technologies). Following RNA extraction, cDNA was synthesised from ADPKD, normal cells and exosomes using specific mir-193b-3p RT primers or a total RNA to cDNA kit (Life Technologies). Real time PCR was carried out on an ABI7900 qPCR machine. Normalisation of expression was carried out using specific primers to *GAPDH* or *RNU44*. Results presented are representative of 3 separate experiments. $Cre;Pkd1^{del2-11,lox}$ mice were generated as previously described (15). RNA was extracted from 4-5 mouse kidneys at 3 months and 4 months after tamoxifen treatment at post-natal day 40, retrotranscribed into cDNA and changes in ErbB4 and mir-193b-3p expression determined. Analysis of gene and miRNA expression were carried out using DataAssist v3.01 (Applied Biosystems) to calculate 1/ΔCt normalised expression values for each cell line. Data was plotted in Graphpad Prism and p-values >0.05 (adjusted for Benjamini-Hochberg False Discovery Rate) were defined as significant. Relative quantification was also carried out using the comparative Ct (ΔΔCt) method to calculate fold changes in expression between control and ADPKD samples.

Small Interfering (siRNA) knockdown

Isoform-specific siRNA to human ErbB4 was chemically synthesized by Cell Signalling Technology. A scrambled negative control siRNA (Silencer) was purchased from Ambion. Transfection of siRNA into cells was achieved using RNAiMax reagent (Life Technologies). Knockdown was confirmed by qPCR 48 h post-transfection.

Immunoblotting

Total cell lysates were prepared and processed for immunoprecipitation and Western blotting as described previously (20). Cells were solubilized in detergent lysis buffer (50 mM Tris, 0.14 M NaCl, 1% Triton X-100, and 0.5% NP40) supplemented with Complete protease inhibitors and PhosStop phosphatase inhibitors (Roche Diagnostics, Mannheim, Germany). Commercial antibodies against the C-terminus of ErbB4 (EP192Y), phosphoErbB4-Y1188 (EPR2271Y) (Abcam, UK), calnexin, pAKT, total AKT, pERK and total ERK (Cell Signalling, USA) were used for western blotting. ECL detection and quantification was carried out using a Biorad Chemidoc XRS+ system running Image Lab automated image capture and analysis software. All quantification was carried out on non-saturated bands as determined by the software. Data is presented as the ratio of ErbB4 to calnexin.

Immunohistochemistry

Archival nephrectomy sections were obtained from 6 ADPKD patients with known truncating *PKD1* mutations and from 3 control patients (22). Mouse kidney tissue from *Cre;Pkd1*$^{del2-11,lox}$ mice were obtained at 1, 2, 3 and 4 months post tamoxifen treatment (n=3). Formalin-fixed paraffin sections were dewaxed and hydrated through graded ethanol solutions. For antigen retrieval, the sections were placed in 10 mM citric acid buffer (pH 6.0) and incubated in a pre-heated water-bath maintained at 95°C for 15 min. Endogenous peroxidase activity was quenched by treatment with methanol containing 3% hydrogen peroxide for 30 m. Sections were then incubated in diluted blocking serum for 30 m, followed by incubation overnight at 4°C with ErbB4 antibody (1:100 dilution). For human and mouse kidney sections, a peroxidase-conjugated secondary antibody was employed and peroxidase activity was visualised using a substrate solution of diaminobenzidine (DAB) containing 0.03% hydrogen peroxide. Negative control sections were processed with omission of the primary antibody and a non-immune IgG. All sections were counterstained in haematoxylin.

Luciferase Reporter Assay

A 428bp fragment of the 3’UTR of ErbB4 containing a predicted mir-193b-3p seed sequence was amplified from RNA extracted from HEK-293 cells by PCR using the following primers:

Forward: GGTCGTGAGCTCCACACCTGCTCCAATTTCCCC

Reverse: CTCGTACTCGAGATGCACACATCAGTTCCTGC

Following reverse transcription, ErbB4 3'UTR cDNA was subcloned into a pmirGLO reporter plasmid (Promega). The predicted mir-193b-3p seed sequence was mutated using the following primers according to the Stratagene site-directed mutagenesis protocol:

Forward: CTTCCTTCTACCCCAAGGCGTCTCGTTTTGACACTTCCCAG

Reverse: CTGGGAAGTGTCAAAACGAAGACGCCTTGGGGTAGAAGGAAG

For the luciferase assay, HEK293 cells were plated into a 96-well plate at 25,000 cells / well the day before transfection. For 5 replicates, 1.5µL of Lipofectamine 2000 reagent was mixed to 50µL of OptiMEM medium and 375µg of pcDNA 3.1 + 125ng pmirGLO vector together with negative control miRNA or a mir-193b-3p mimic at a final concentration of 25 or 50 nM. 24 h after transfection, the luciferase/renilla signals ratios were measured using the Dual Luciferase Reporter Assay from Promega. 100 µL of Passive Lysis Buffer was added directly into the wells to lysate the cells and 50 µL from each well were used for signal detection with a Perkin Elmer luminometer.

ErbB4 functional inhibition assays

Control and ADPKD cells were plated at 5000 cells/well in a 96well plate. Cells were incubated with a pan-ErbB inhibitor including to ErbB4, JNJ 28871063 hydrochloride (Tocris, USA) for 24 h, an inhibitory ErbB4 antibody (clone H.72.8, Millipore, USA) or non-immune control rabbit antibody for 72 h. To test the effect of the ErbB4 ligand NRG-1, cells were serum starved for 24 h prior to incubation with 100 ng/ml NRG-1 (Cell Signalling, USA) for 72 h. Following the indicated treatment, cell proliferation was measured using a commercial BrdU ELISA kit (Roche, Basel, Switzerland) according to the manufacturer's instructions.

Matrigel 3D cyst assays

OX161 cells (1x10^5/well) were mixed with 70 µl Matrigel (Becton Dickinson, UK), plated into 96 well plates in triplicate and incubated for 30 m at 37°C to allow the gel to set. Cells were cultured for 12 d in the presence or absence of 100 ng/ml NRG-1 or HB-EGF. Media was replaced every 2 d. The average cyst area was calculated by measuring cyst areas in individual wells on days 4, 7 and 12. At least 65 cysts were measured in triplicate wells at each time-point.

Patient recruitment

All participants gave their signed informed consent at the time of recruitment. ADPKD patients were recruited through the Sheffield Kidney Institute and healthy normal volunteers were recruited from laboratory staff. Ethical approval for this study was obtained from the National Research Ethics Service Committee Yorkshire & The Humber - Bradford (REC12/YH/0297). Following collection, urine samples were centrifuged at 1000g for 10 min at 4^{o}C. Cell pellets were discarded and cell free supernatants stored at -80^{o}C until further analysis.

Isolation of Urinary Extracellular Vesicles

Urinary extracellular vesicles (UEVs) or exosomes were isolated by differential centrifugation as previously reported (25). In brief, 10 ml of urine was initially centrifuged at 17000g for 15 min. The supernatant was retained and the pellet resuspended in 200 µl isolation buffer (250 mM Sucrose, 10 mM Triethanolamine pH7.6, 50 µl of DDT) to reduce the highly abundant Tamm-Horsfall protein. Following incubation at room temperature for 5 min, the sample was briefly vortexed and centrifuged again at 17,000g for 15 min. This supernatant was then combined with the initial supernatant and centrifuged once more at 170000 g for 150 min. The final pellet was re-suspended in 50 µl lysis buffer (50 mM Tris pH 7.4, 150 mM sodium chloride, 1% Triton X-100, 1% sodium-deoxycholic acid and protease inhibitors) on ice for 1 h (3). A protein assay was carried out to normalise protein concentration prior to SDS-PAGE.

Electron Microscopy

Electron microscopy was carried out to visualize the morphology of the UEVS isolated. Briefly, the pellet isolated was first resuspended in 50 µl PBS and a small drop of this mixture was deposited on 200-mesh nickel grids. Negative staining of the mesh was carried out using heavy metal salt (0.5 % Uranium). After drying, the nickel grids were visualized using a Philips electron microscope 400 operated at 80 KV.

Statistical Analysis

Data are presented as mean values ± SEM. Student's *t* test or ANOVA were used for statistical analysis with a p value of <0.05 indicating statistical significance. The degree of significance as determined by GraphPad Prism software is denoted by the following asterisks: $*P \leq 0.05$, $**P \leq 0.01$, $***P \leq 0.001$, $****P \leq 0.0001$

Results

Parallel mRNA/miRNA expression microarray profiling in ADPKD cell lines

A parallel mRNA and miRNA expression microarray was performed to identify differential changes in mRNA/miRNA expression levels in ADPKD cells compared to non-ADPKD controls. We then used this information to identify predicted mRNA/miRNA interactions which could contribute to ADPKD pathogenesis (**Fig 1A**). The expression of 1515 genes was significantly altered between control and ADPKD cell lines by more than 2 fold and 5 miRNAs were significantly altered. In total, 447 genes were significantly up-regulated (**Fig 2A**) and 1068 genes (**Fig 2B**) significantly down-regulated in ADPKD cells. All the significantly altered miRNAs were down-regulated in ADPKD cells (**Fig 2C**). These miRNAs in turn were predicted to target 5721 genes (TargetScan algorithm) of which 390 genes were differentially expressed in the parallel mRNA microarray. Functional enrichment analysis of differentially expressed genes (>2 fold) in ADPKD was carried out using Panther pathway analysis software (http://www.pantherdb.org/). A total of 22 signalling pathways were significantly enriched from the list of genes upregulated in ADPKD whereas 8 pathways were significantly enriched from the list of genes downregulated in ADPKD (**Fig 1B**). These included pathways reported to be associated with ADPKD including cadherin, EGF receptor (3.38 fold enrichment), Wnt and G protein signalling. Of the ErbB receptors, the only receptor showing significant differential expression was ErbB4 (~40-fold).

Validation of an interaction between mir-193b-3p and ErbB4 mRNA

The differential increase in ErbB4 expression was first confirmed by Taqman qPCR, showing a mean 10-fold increase in ADPKD compared to control cells (**Fig 3A**). We noted that of the

5 differentially expressed miRNA identified, mir-193b-3p was predicted to regulate ErbB4, this also being the highest ranked gene identified by a TargetScan prediction algorithm (http://www.targetscan.org/, Release 6.2) of 30 predicted targets (**Fig 2D**). Consistent with these predictions, multiple independent miRNA target prediction algorithms (DIANAmT, miRanda, miRDB, miRWalk, RNAhybrid, Targetscan and PICTAR5) identified two potential mir-193b-3p binding sites within the 3'UTR of ErbB4.

We next validated the reduction of array mir-193b-3p expression in ADPKD cells by Taqman qPCR showing a 0.5 fold decrease (**Fig 3B**). To provide direct evidence of a functional interaction between mir-193b-3p and ErbB4 mRNA, we generated a luciferase reporter plasmid (pmirGLO) containing a fragment of the ErbB4 3'UTR and mutated the predicted mir-193b-3p seed sequence in a second reporter construct (**Fig 3C**). Co-expression of a mir-193b-3p miRNA mimic significantly reduced luciferase activity in the wild-type but had no effect on the mutated sequence (**Fig 3D**). Finally, expression of the mir-193b-3p mimic in the ADPKD cell line (OX161) resulted in a significant reduction in endogenous ErbB4 mRNA (**Fig 3E**) and ErbB4 protein (**Fig 3F**). These results provide the first evidence that ErbB4 mRNA is potentially a target of mir-193b-3p.

ErbB4 is over-expressed in ADPKD cell lines as two distinct isoforms

By immunoblotting, we confirmed that full-length ErbB4 protein were increased in all four ADPKD cell lines tested, being almost undetectable in control cells (**Fig 4A**). The *ERBB4* gene however is known to undergo alternative splicing generating several isoforms differing in their N-termini or C-termini (**Fig 4B**). For instance, the two CYT isoforms differ in a stretch of 16 amino acids in the C-terminus encoded by a single exon (CYT-1) that is absent in CYT-2. This structural difference contributes to differential subcellular targeting and even antagonistic functional responses mediated by the two CYT isoforms (40). Apart from the CYT isoforms, tissue-specific alternative splicing can generate JM-a and JM-b isoforms differing in their extracellular juxta-membrane (JM) domain and function (6).

To investigate the possibility of an isoform switch in ADPKD, RT-PCR was carried out using specific primers flanking the variable regions using cDNA isolated from OX161 cells (**Fig 4B**). As a positive control, we used a JM-a/CYT-1 plasmid. For the JM region, the expected sizes were 0.375kb (JM-a) and 0.345kb (JM-b) respectively. A single band corresponding to JM-a (0.375kb) was detected with no evidence of JM-b (0.345kb) (**Fig 4C**). Similar analysis using primers flanking the cytoplasmic site revealed that both CYT-1 and CYT-2 isoforms were expressed, with a higher abundance of CYT-1. Primers designed to a conserved ErbB4 motif identified the same control band in both samples. Our results reveal the presence of two isoforms (JM-a/CYT-1 and JM-a/CYT-2) in normal and ADPKD cells with no evidence of an isoform switch (**Fig 4D**).

Nuclear ErbB4 expression is increased in human ADPKD kidneys and in a *Pkd1* mouse model

The expression of ErbB4 was increased in cyst lining epithelial cells of human ADPKD kidney sections compared to control kidney tissue by immunohistochemistry (**Fig 4E**). Significantly elevated nuclear localisation of ErbB4 was observed in ErbB4 positive cysts (black arrows) indicating increased levels of ErbB4 protein and C-terminal cleavage (**Fig 4E, F**). We next analysed ErbB4 expression in a previously reported inducible kidney-specific Pkd1 mutant mouse model (14). Following induction with tamoxifen at PN40 these animals slowly develop a cystic phenotype with large cysts becoming apparent 4 months after tamoxifen induction. In agreement with the human studies, there was a significant increase in

ErbB4 mRNA expression in *Cre;Pkd1*$^{del2-11,lox}$ mice induced with Tamoxifen at 4 months (**Fig 4G**). Similarly, ErbB4 staining was increased in cyst lining epithelial cells of kidney sections. The number of ErbB4 positive cysts increased following Pkd1 deletion with the strongest staining at 4 months after tamoxifen induction. (**Fig 4H**) In agreement elevated nuclear localisation in ErbB4 positive cysts was significant from 2 months after induction (**Fig 4I**). In both human and mouse tissue sections a minority of cysts (~20%) showed no detectable ErbB4 staining although it was not possible to distinguish these from positive stained cysts in terms of size or time following induction. At 4 months, a significant decrease in mir-193b-3p mRNA was detectable in *Cre;Pkd1*$^{del2-11,lox}$ kidneys (**Fig 4J**).

Increased expression of cleaved ErbB4 and decreased expression of mir-193b-3p in human ADPKD urinary extracellular vesicles

To confirm that these changes also occurred *in vivo*, we isolated urinary extracellular vesicles (UEV) from healthy volunteers (n=12) and ADPKD patients with early (eGFR >60ml/min/1.73m^2, n=16) or late disease (eGFR <60ml/min/1.73m^2, n=16) using an established protocol (25). Electron microscopy confirmed the presence of multiple (<100nm) vesicles in the pelleted fraction (**Fig 5A**). The exosome-specific protein TSG-101 was restricted to the pellet and there was clear expression of aquaporin-2 (AQP2) in both cell-free urine and the pellet indicating the origin of some vesicles from collecting ducts (**Fig 5B**).

An ErbB4 positive band was detected at 80 kDa in UEVs, corresponding to the known C-terminal intracellular domain (ICD) generated by γ-secretase mediated cleavage (**Fig 5C**). A minor band at 50 kDa was also observed which could correspond to proteolytic degradation or represent a non-specific band. Expression of the 80kDa band was significantly increased in the UEVs of ADPKD patients compared to healthy controls particularly in patients with late disease as defined by baseline eGFR (**Fig 5D**). ErbB4 expression also correlated significantly with the rate of decline in eGFR and outperformed mean kidney length (MKL) measured by ultrasound (**Fig 5E**). In combination, ErbB4 and MKL were additive in ROC analysis, accounting for 0.816 of AUC (p=0.002).

Increased ligand dependent proliferation signalling and cyst growth in ADPKD cells

A total of 11 ligands have been reported to bind to members of the EGF receptor family. Of these, several have been shown to activate ErbB4 including the neuregulins (NRG1-4) and HB-EGF (27). However, ErbB4 activation can stimulate or inhibit proliferation in different cells, possibly due to differential expression of ErbB4 isoforms (37, 40).

To determine the functional consequence of ErbB4 overexpression in ADPKD cells, we first studied their response to NRG-1. A significant increase in NRG-1 mediated proliferation was seen in the *PKD1* cell lines with almost no effect in control cells (**Fig 6A**). This was mirrored by significant increases in phosphorylated ErbB4 (pErbB4) in response to NRG-1 (**Fig 6B**). Since the OX161 line showed the greatest response to NRG-1, this line was used for further experiments.

The JM-a isoforms of ErbB4 are known to undergo two step-wise proteolytic cleavage events when activated, generating a shed N-terminal ectodomain (110kDa) by Tumour Necrosis Factor Alpha Converting Enzyme (TACE) cleavage and a soluble intracellular C-terminal domain (80kDa) by the action of γ-secretase (17). Several downstream signalling pathways are known to be activated including the PI3K/AKT pathway (cell survival), STAT 5 (mammary development), Ras/ERK1/2 and PLCγ pathways (cell proliferation). Accordingly, a significantly greater increase in pERK and pAKT was observed in ADPKD (OX161) cells in response to NRG-1 compared to control (UCL93) cells (**Fig 6C**).

A small single centre study recently reported that urinary HB-EGF excretion was increased in a cohort of ADPKD patients and showed a positive correlation with more advanced disease ie lower GFR and higher total kidney volumes (10). In contrast, urinary EGF and TGF-α levels decreased with increasing disease severity. Incubation with HB-EGF, similar to NRG-1, was associated with an increase in phosphorylated ErbB4 in ADPKD cells (OX161) suggesting a potential role in activating ErbB4 in ADPKD cells (**Fig 6D**). The effect of both ErbB4 ligands on cyst growth was therefore studied in 3D cyst assays. OX161 cells spontaneously form cyst-like structures with well-developed lumen when cultured in matrigel. Both NRG-1 and HB-EGF significantly increased cyst growth in OX161 cells as measured by total cyst area in 3D cyst assays (**Fig 6E**). These results confirm that ligand-activated ErbB4 signalling is likely to be a pathogenic factor in ADPKD cyst expansion, by promoting cell survival and stimulating cell proliferation.

Inhibition of ErbB4 reduces proliferation in ADPKD cells

Over-expression of ErbB4 in control (UCL93) cells significantly increased basal cell proliferation showing that increasing ErbB4 expression alone was sufficient to induce a pro-proliferative phenotype (**Fig 7A)**. Conversely, siRNA knockdown of ErbB4 in OX161 cells inhibited cell proliferation compared to control siRNA treated cells (**Fig 7B, C**).

A pan-ErbB inhibitor (JNJ 28871063) which inhibits ErbB1, ErbB2 and ErbB4 (IC_{50} 21-38 nM) (7) reduced proliferation of OX161 cells but had no effect on UCL93 cells at the same doses (**Fig 7D**). These results are consistent with the specificity of JNJ 28871063 on ErbB-driven cancer cell lines but its lack of effect in non-ErbB lines (7).

Although ErbB1, ErbB2 and ErbB3 were not differentially expressed in the ADPKD cells, we decided to utilise an ErbB4-specific inhibitory antibody to isolate an ErbB4 specific role in these cells (12, 29, 39). ErbB4 selective blockade reduced basal proliferation in OX161 cells to that seen in UCL93 control cells (**Fig 7E**) whereas an irrelevant IgG control antibody had no effect (**Fig 7F**). These results demonstrate that ErbB4 activation could contribute to the increased proliferation rate of ADPKD cells, probably through the action of endogenous ligands such as NRG1 and HB-EGF.

Discussion

In this paper, we report the identification of ErbB4 as a potential new biomarker of disease activity and a new therapeutic target in ADPKD. Parallel discovery microarray profiling in a panel of human ADPKD cell lines previously shown to express germline and somatic mutations in *PKD1* but not *PKD2* (24) identified a total of 1513 differentially expressed genes in ADPKD cells mapping to several pathways previously implicated in ADPKD. We also identified 5 miRNAs that were significantly down regulated in ADPKD cells.

The EGF/ErbB receptor family has been previously implicated in experimental models of ADPKD (11). The ErbB receptor family has four members: EGFR/ErbB1, ErbB2/HER2/neu, ErbB3/HER3 and ErbB4/HER4 which belong to the receptor tyrosine kinase superfamily. A total of 11 putative ligands with different receptor selectivity to the ErbB receptors have been reported, with the exception of ErbB2 (27). The complexity of EGF/ErbB signalling is further compounded by the formation of different homo- and heterodimers and the existence of multiple splice forms (especially for ErbB4).

The role of EGF/ErbB signalling in ADPKD pathogenesis has attracted attention due to the hyperproliferative phenotype that characterises ADPKD (1). However, inhibition of EGF signalling has yielded conflicting results in different experimental models. For instance, an EGFR and ErbB2 antagonist reduced cystic disease in the Han:SPRD rat and bpk mouse models but had a detrimental effect in the Pck rat (26, 32, 34, 35). Nonetheless, the physiological importance of the EGF receptor during kidney development, repair and tubular physiology could make this a difficult drug target for ADPKD.

We decided to focus our study on ErbB4 for a number of reasons. In murine PKD disease models, renal ErbB4 expression has been shown to be increased (*bpk*, *cpk*) (19, 42). ErbB4 plays a key role during nephrogenesis being induced in the earliest murine tubular structures by E14.5 and later in the collecting ducts (37). ErbB4 null mice die by E11 prior to nephrogenesis due to defective heart development (9) but ErbB4 knockout mice rescued with a cardiac myosin-promoter driven ErbB4 transgene have defective mammary gland and neuronal abnormalities but no reported kidney phenotype and display a normal lifespan (33). Consistent with a major role during development, conditional deletion (Pax8-Cre) of ErbB4 affecting both renal ErbB4 isoforms (JMa-CYT-1, JMa-CYT-2) from E11.5 altered normal tubular diameter, cell number and differentiation (37). Conversely, transgenic expression of JMa-CYT-2 in the kidney from E11.5 resulted in cortical cysts, tubular proliferation and lumen dilatation (37). Unexpectedly, another group reported that deletion of ErbB4 significantly worsened the cystic phenotype of *cpk* mice, a recessive model of PKD (42). One possible explanation for this discrepancy is that both major ErbB4 isoforms were deleted in this study. While deletion of JMa-CYT-2 should be protective (see below), deletion of the JMa-CYT-1 isoform could enhance cystogenesis by removing an inhibitory brake on cell proliferation; the differential expression of each ErbB4 isoform in the kidneys of *cpk* mice was not reported. This imbalance created by deleting both ERbB4 isoforms could have resulted in the surprising results observed in *cpk*/ErbB4 null mice. Formal testing of these possibilities in orthologous models by chemical or genetic manipulation will be required to obtain a definitive answer relevant to ADPKD.

We observed a consistent upregulation of ErbB4 expression in human and mouse disease models, both *in vitro* and *in vivo*. In addition, we report for the first time that ErbB4 is a direct target for mir-193b-3p. The increase in ErbB4 mRNA occurs early in disease (2 months in Pkd1 conditional mice, Fig 4G) and is likely to involve increased gene transcription in view of the magnitude of ErbB4 elevation (10-fold) observed in cells. At a later stage of disease, it is probable that the reduction in mir-193b-3p expression also contributes to a post-transcriptional increase in ErbB4 mRNA levels (Fig 4G, J).

In the kidney, ErbB4 is expressed predominantly as the isoforms JM-a/CYT-1 and JM-a/CYT-2, with possibly more medullary expression of JM-a/CYT-2 (37, 44). Both isoforms undergo sequential proteolytic cleavage to generate a soluble intracellular domain (ICD) that can translocate to the nucleus to regulate gene transcription. The CYT-1 isoform contains a 16 aa sequence which is lacking in the CYT-2 isoform, enabling CYT-1 to couple to PI3K. However, levels of kinase activity, protein stability and nuclear accumulation are greater for the CYT-2 ICD than the CYT-1 ICD (30, 43). CYT-1 ICD inhibits cell proliferation, undergoes ubiquitination but promotes cell differentiation whereas the opposite is true for the CYT-2 ICD (18, 31, 38, 40). Both isoforms were similarly expressed in control and ADPKD cells with a slightly greater expression of CYT-1.

The increase in ErbB4 expression was also associated with increased ligand-activated signalling. Addition of two ErbB4 ligands, NRG-1 and HB-EGF, was associated with increased ErbB4 phosphorylation, downstream activation of pERK and pAKT pathways, increased proliferation and cyst formation in ADPKD cells. Conversely, blocking endogenous ErbB4 in cystic cells using siRNA, a kinase inhibitor (JNJ288) or an anti-functional antibody (H.72.8) reduced cell proliferation to that of untreated controls. These findings were confirmed by evidence of increased ErbB4 activation *in vivo*. Cystic human and murine kidney sections showed increased nuclear expression of C-terminal ErbB4. Finally, we detected increased levels of cleaved C-terminal ErbB4 in human ADPKD UEVs compared to healthy controls. ErbB4 expression was significantly raised in patients with reduced kidney function (eGFR>60ml/min/1.73m^2) and in ROC analysis, was significantly correlated with a more rapid rate of eGFR decline (>3ml/min/pa), outperforming ultrasound-measured mean kidney length. These findings suggest that ErbB4 signalling closely parallels disease activity and could represent a prognostic biomarker of disease progression.

Our results point to the possibility of targeting ErbB4 to retard cyst growth and disease progression in ADPKD. This could be done at several levels or in combination eg blocking the ligands such as NRG-1 or HB-EGF, targeting ErbB4 itself through anti-functional antibodies (12, 29, 39), reducing its expression through mir-193b-3p mimics (5, 28, 36, 41) or through inhibiting downstream kinase activity with selective small molecule inhibitors. Previous studies have detected a significant increase in NRG-1 (2, 23) or HB-EGF (13) in *Pkd1* cystic kidneys and increased urinary HB-EGF has been detected in human ADPKD (10). Of interest, it was reported in the same study that treatment with the vasopressin V2 receptor antagonist (V2RA), tolvaptan, was associated with a significant increase in urinary HB-EGF (10). This simultaneous upregulation of HB-EGF could mean that treatment with tolvaptan is less effective than would be predicted from its effect on cAMP production. Therefore, combining a V2RA with a therapy which blocks ErbB4 signalling could be potentially synergistic.

Acknowledgements

TAM was supported by a PhD scholarship from the Libyan Government. RJS was supported by an NIHR Clinical Lectureship. We thank Mike O'Hare, Fiona Wright, Paul Heath, Wouter Leonhard and Bart Wagner for technical advice and assistance.

Grants

Research Councils UK, University of Sheffield, ERA-EDTA Working Group on Inherited Kidney Diseases, Sheffield Kidney Research Foundation and the European Union (EU-FP7/2007-2013, grant agreement no. 317246, TranCYST).

References

1. **Chang MY, Parker E, Ibrahim S, Shortland JR, Nahas ME, Haylor JL, and Ong AC**. Haploinsufficiency of Pkd2 is associated with increased tubular cell proliferation and interstitial fibrosis in two murine Pkd2 models. *Nephrol Dial Transplant* 21: 2078-2084, 2006.

2. **Chen WC, Tzeng YS, and Li H**. Gene expression in early and progression phases of autosomal dominant polycystic kidney disease. *BMC Res Notes* 1: 131, 2008.

3. **Cheng L, Sharples RA, Scicluna BJ, and Hill AF**. Exosomes provide a protective and enriched source of miRNA for biomarker profiling compared to intracellular and cell-free blood. *J Extracell Vesicles* 3: 2014.

4. **Cornec-Le Gall E, Audrezet MP, Chen JM, Hourmant M, Morin MP, Perrichot R, Charasse C, Whebe B, Renaudineau E, Jousset P, Guillodo MP, Grall-Jezequel A, Saliou P, Ferec C, and Le Meur Y**. Type of PKD1 mutation influences renal outcome in ADPKD. *J Am Soc Nephrol* 24: 1006-1013, 2013.

5. **Di Martino MT, Leone E, Amodio N, Foresta U, Lionetti M, Pitari MR, Cantafio ME, Gulla A, Conforti F, Morelli E, Tomaino V, Rossi M, Negrini M, Ferrarini M, Caraglia M, Shammas MA, Munshi NC, Anderson KC, Neri A, Tagliaferri P, and Tassone P**. Synthetic miR-34a mimics as a novel therapeutic agent for multiple myeloma: in vitro and in vivo evidence. *Clin Cancer Res* 18: 6260-6270, 2012.

6. **Elenius K, Corfas G, Paul S, Choi CJ, Rio C, Plowman GD, and Klagsbrun M**. A novel juxtamembrane domain isoform of HER4/ErbB4. Isoform-specific tissue distribution and differential processing in response to phorbol ester. *J Biol Chem* 272: 26761-26768, 1997.

7. **Emanuel SL, Hughes TV, Adams M, Rugg CA, Fuentes-Pesquera A, Connolly PJ, Pandey N, Moreno-Mazza S, Butler J, Borowski V, Middleton SA, Gruninger RH, Story JR, Napier C, Hollister B, and Greenberger LM**. Cellular and in vivo activity of

JNJ-28871063, a nonquinazoline pan-ErbB kinase inhibitor that crosses the blood-brain barrier and displays efficacy against intracranial tumors. *Mol Pharmacol* 73: 338-348, 2008.

8. **Gansevoort RT, Arici M, Benzing T, Birn H, Capasso G, Covic A, Devuyst O, Drechsler C, Eckardt KU, Emma F, Knebelmann B, Le Meur Y, Massy ZA, Ong AC, Ortiz A, Schaefer F, Torra R, Vanholder R, Wiecek A, Zoccali C, and Van Biesen W**. Recommendations for the use of tolvaptan in autosomal dominant polycystic kidney disease: a position statement on behalf of the ERA-EDTA Working Groups on Inherited Kidney Disorders and European Renal Best Practice. *Nephrol Dial Transplant* 31: 337-348, 2016.

9. **Gassmann M, Casagranda F, Orioli D, Simon H, Lai C, Klein R, and Lemke G**. Aberrant neural and cardiac development in mice lacking the ErbB4 neuregulin receptor. *Nature* 378: 390-394, 1995.

10. **Harskamp LR, Gansevoort RT, Boertien WE, van Oeveren W, Engels GE, van Goor H, and Meijer E**. Urinary EGF Receptor Ligand Excretion in Patients with Autosomal Dominant Polycystic Kidney Disease and Response to Tolvaptan. *Clin J Am Soc Nephrol* 10: 1749-1756, 2015.

11. **Harskamp LR, Gansevoort RT, van Goor H, and Meijer E**. The epidermal growth factor receptor pathway in chronic kidney diseases. *Nat Rev Nephrol* 12: 496-506, 2016.

12. **Hollmen M, Maatta JA, Bald L, Sliwkowski MX, and Elenius K**. Suppression of breast cancer cell growth by a monoclonal antibody targeting cleavable ErbB4 isoforms. *Oncogene* 28: 1309-1319, 2009.

13. **Jiang ST, Chiou YY, Wang E, Lin HK, Lin YT, Chi YC, Wang CK, Tang MJ, and Li H**. Defining a link with autosomal-dominant polycystic kidney disease in mice with congenitally low expression of Pkd1. *Am J Pathol* 168: 205-220, 2006.

14. **Lantinga-van Leeuwen IS, Leonhard WN, van der Wal A, Breuning MH, de Heer E, and Peters DJ**. Kidney-specific inactivation of the Pkd1 gene induces rapid cyst formation in developing kidneys and a slow onset of disease in adult mice. *Hum Mol Genet* 16: 3188-3196, 2007.

15. **Leonhard WN, van der Wal A, Novalic Z, Kunnen SJ, Gansevoort RT, Breuning MH, de Heer E, and Peters DJ**. Curcumin inhibits cystogenesis by simultaneous interference of multiple signaling pathways: in vivo evidence from a Pkd1-deletion model. *Am J Physiol Renal Physiol* 300: F1193-1202, 2011.

16. **Mao Z, Chong J, and Ong AC**. Autosomal dominant polycystic kidney disease: recent advances in clinical management. *F1000Res* 5: 2029, 2016.

17. **Muraoka-Cook RS, Sandahl M, Husted C, Hunter D, Miraglia L, Feng SM, Elenius K, and Earp HS, 3rd**. The intracellular domain of ErbB4 induces differentiation of mammary epithelial cells. *Mol Biol Cell* 17: 4118-4129, 2006.

18. **Muraoka-Cook RS, Sandahl MA, Strunk KE, Miraglia LC, Husted C, Hunter DM, Elenius K, Chodosh LA, and Earp HS, 3rd**. ErbB4 splice variants Cyt1 and Cyt2 differ by 16 amino acids and exert opposing effects on the mammary epithelium in vivo. *Mol Cell Biol* 29: 4935-4948, 2009.

19. **Nemo R, Murcia N, and Dell KM**. Transforming growth factor alpha (TGF-alpha) and other targets of tumor necrosis factor-alpha converting enzyme (TACE) in murine polycystic kidney disease. *Pediatr Res* 57: 732-737, 2005.

20. **Newby LJ, Streets AJ, Zhao Y, Harris PC, Ward CJ, and Ong AC**. Identification, characterization, and localization of a novel kidney polycystin-1-polycystin-2 complex. *J Biol Chem* 277: 20763-20773, 2002.

21. **Ong AC, Devuyst O, Knebelmann B, Walz G, and Diseases E-EWGfIK**. Autosomal dominant polycystic kidney disease: the changing face of clinical management. *Lancet* 385: 1993-2002, 2015.

22. **Ong AC, Ward CJ, Butler RJ, Biddolph S, Bowker C, Torra R, Pei Y, and Harris PC**. Coordinate expression of the autosomal dominant polycystic kidney disease proteins, polycystin-2 and polycystin-1, in normal and cystic tissue. *Am J Pathol* 154: 1721-1729, 1999.

23. **Pandey P, Qin S, Ho J, Zhou J, and Kreidberg JA**. Systems biology approach to identify transcriptome reprogramming and candidate microRNA targets during the progression of polycystic kidney disease. *BMC Syst Biol* 5: 56, 2011.

24. **Parker E, Newby LJ, Sharpe CC, Rossetti S, Streets AJ, Harris PC, O'Hare MJ, and Ong AC**. Hyperproliferation of PKD1 cystic cells is induced by insulin-like growth factor-1 activation of the Ras/Raf signalling system. *Kidney Int* 72: 157-165, 2007.

25. **Pisitkun T, Shen RF, and Knepper MA**. Identification and proteomic profiling of exosomes in human urine. *Proc Natl Acad Sci U S A* 101: 13368-13373, 2004.

26. **Richards WG, Sweeney WE, Yoder BK, Wilkinson JE, Woychik RP, and Avner ED**. Epidermal growth factor receptor activity mediates renal cyst formation in polycystic kidney disease. *J Clin Invest* 101: 935-939, 1998.

27. **Riese DJ, 2nd, and Stern DF**. Specificity within the EGF family/ErbB receptor family signaling network. *Bioessays* 20: 41-48, 1998.

28. **Roberts TC, and Wood MJ**. Therapeutic targeting of non-coding RNAs. *Essays Biochem* 54: 127-145, 2013.

29. **Starr A, Greif J, Vexler A, Ashkenazy-Voghera M, Gladesh V, Rubin C, Kerber G, Marmor S, Lev-Ari S, Inbar M, Yarden Y, and Ben-Yosef R**. ErbB4 increases the proliferation potential of human lung cancer cells and its blockage can be used as a target for anti-cancer therapy. *Int J Cancer* 119: 269-274, 2006.

30. **Sundvall M, Peri L, Maatta JA, Tvorogov D, Paatero I, Savisalo M, Silvennoinen O, Yarden Y, and Elenius K**. Differential nuclear localization and kinase activity of alternative ErbB4 intracellular domains. *Oncogene* 26: 6905-6914, 2007.

31. **Sundvall M, Veikkolainen V, Kurppa K, Salah Z, Tvorogov D, van Zoelen EJ, Aqeilan R, and Elenius K**. Cell death or survival promoted by alternative isoforms of ErbB4. *Mol Biol Cell* 21: 4275-4286, 2010.

32. **Sweeney WE, Chen Y, Nakanishi K, Frost P, and Avner ED**. Treatment of polycystic kidney disease with a novel tyrosine kinase inhibitor. *Kidney Int* 57: 33-40, 2000.

33. **Tidcombe H, Jackson-Fisher A, Mathers K, Stern DF, Gassmann M, and Golding JP**. Neural and mammary gland defects in ErbB4 knockout mice genetically rescued from embryonic lethality. *Proc Natl Acad Sci U S A* 100: 8281-8286, 2003.

34. **Torres VE, Sweeney WE, Jr., Wang X, Qian Q, Harris PC, Frost P, and Avner ED**. EGF receptor tyrosine kinase inhibition attenuates the development of PKD in Han:SPRD rats. *Kidney Int* 64: 1573-1579, 2003.

35. **Torres VE, Sweeney WE, Jr., Wang X, Qian Q, Harris PC, Frost P, and Avner ED**. Epidermal growth factor receptor tyrosine kinase inhibition is not protective in PCK rats. *Kidney Int* 66: 1766-1773, 2004.

36. **Trang P, Wiggins JF, Daige CL, Cho C, Omotola M, Brown D, Weidhaas JB, Bader AG, and Slack FJ**. Systemic delivery of tumor suppressor microRNA mimics using a neutral lipid emulsion inhibits lung tumors in mice. *Mol Ther* 19: 1116-1122, 2011.

37. **Veikkolainen V, Naillat F, Railo A, Chi L, Manninen A, Hohenstein P, Hastie N, Vainio S, and Elenius K**. ErbB4 modulates tubular cell polarity and lumen diameter during kidney development. *J Am Soc Nephrol* 23: 112-122, 2012.

38. **Veikkolainen V, Vaparanta K, Halkilahti K, Iljin K, Sundvall M, and Elenius K**. Function of ERBB4 is determined by alternative splicing. *Cell Cycle* 10: 2647-2657, 2011.

39. **Vexler A, Lidawi G, Loew V, Barnea I, Karaush V, Lev-Ari S, Shtabsky A, and Ben-Yosef R**. Anti-ERBb4 targeted therapy combined with radiation therapy in prostate cancer. Results of in vitro and in vivo studies. *Cancer Biol Ther* 7: 1090-1094, 2008.

40. **Wali VB, Gilmore-Hebert M, Mamillapalli R, Haskins JW, Kurppa KJ, Elenius K, Booth CJ, and Stern DF**. Overexpression of ERBB4 JM-a CYT-1 and CYT-2 isoforms in transgenic mice reveal isoform-specific roles in mammary gland development and carcinogenesis. *Breast Cancer Res* 16: 501, 2014.

41. **Xue W, Dahlman JE, Tammela T, Khan OF, Sood S, Dave A, Cai W, Chirino LM, Yang GR, Bronson R, Crowley DG, Sahay G, Schroeder A, Langer R, Anderson DG, and Jacks T**. Small RNA combination therapy for lung cancer. *Proc Natl Acad Sci U S A* 111: E3553-3561, 2014.

42. **Zeng F, Miyazawa T, Kloepfer LA, and Harris RC**. Deletion of ErbB4 accelerates polycystic kidney disease progression in cpk mice. *Kidney Int* 86: 538-547, 2014.

43. **Zeng F, Xu J, and Harris RC**. Nedd4 mediates ErbB4 JM-a/CYT-1 ICD ubiquitination and degradation in MDCK II cells. *FASEB J* 23: 1935-1945, 2009.

44. **Zeng F, Zhang MZ, Singh AB, Zent R, and Harris RC**. ErbB4 isoforms selectively regulate growth factor induced Madin-Darby canine kidney cell tubulogenesis. *Mol Biol Cell* 18: 4446-4456, 2007.

Figure Legends

Fig 1. Parallel mRNA/miRNA expression microarray profiling in ADPKD cell lines

(A) Systematic workflow used to analyse parallel mRNA/miRNA changes between control (n=2) and ADPKD derived cystic cell lines (n=4). **(B)** Pathway enrichment analysis was carried out on the 1515 significantly altered ($p<0.05$ by TTest) genes which were up or down regulated by >2 fold in ADPKD cell lines using the Panther classification system (http://www.pantherdb.org/).

Fig 2. Differential expression of mRNAs and miRNAs in ADPKD cystic cell lines

(A). Differential expression of the top 30 genes up-regulated in ADPKD cell lines expressed as a heatmap. The heatmap was produced by clustering the data matrix of the top 30 genes in GenespringX (Agilent, USA). Analysis of differential expression by TTest was carried out using Agilent GeneSpring GX software and p-values >0.05 were defined as significant. (**B).** Differential expression of the top 30 genes down-regulated in ADPKD cell lines expressed as a heatmap. The heatmap was produced by clustering the data matrix of the top 30 genes in GenespringX (Agilent, USA). Analysis of differential expression by TTest was carried out using Agilent GeneSpring GX software and p-values >0.05 were defined as significant. (**C).** Differential expression of the 5 significantly altered miRNAs in ADPKD cell lines expressed as a heatmap. The heatmap was produced by clustering the data matrix of the altered miRNAs in GenespringX (Agilent, USA). Analysis of differential expression by TTest was carried out using Agilent GeneSpring GX software and p-values >0.05 were defined as significant. (**D).** Differential expression of the top 30 genes predicted to be targets of mir-193b-3p by Targetscan algorithm which were up-regulated in ADPKD cell lines expressed as a heatmap. The heatmap was produced by clustering the data matrix of the top 30 genes in GenespringX (Agilent, USA).

Fig 3. ErbB4 expression is increased in ADPKD cells and is a direct target for mir-193b-3p

(A) Taqman qPCR assays for ErbB4 show a significant increase in expression of transcript in ADPKD derived cell lines (n=4) compared to control cell lines (n=4) representing a 10-fold change relative to control. **(B)** Taqman qPCR assays for mir-193b-3p show a significant reduction in expression of transcript in ADPKD derived cell lines (n=4) compared to control cell lines (n=4) representing a fold change of 0.5066 relative to control. (**C**) Identification of the sequence within the 3'UTR of ErbB4 between nt91-98 recognised by the mir-193b-3p seed sequence CCGGUCA. The 3 base pairs in ErbB4 predicted to disrupt binding of mir-193b-3p and which were mutated are shown in italics. **(D)** ErbB4 (pmirGLO ErbB4) or mutated ErbB4 3'UTR (pmirGLO mErbB4) was cloned into a pmirGLO luciferase reporter vector and transfected into HEK-293 cells. HEK-293 cells were co-transfected with control or mir-193b-3p miRNA mimics at 20 and 50nM. A significant reduction in luciferase activity was seen in cells transfected with ErbB4 3'UTR and a mir-193b-3p mimic but not in cells transfected with mutated ErbB4 3'UTR. A negative non-targeting miRNA control mimic had no effect on luciferase activity. **(E)** Taqman qPCR assays for ErbB4 show a significant decrease in expression of the endogenous mRNA transcript in OX161 cells when transfected with 50nM mir-193b mimic (n=3) relative to cells transfected with 50 nM scrambled negative control mimic (n=3) representing a fold change of 0.6207 relative to control. **(F)** Transfection of HEK-293 cells with a mir-193b-3p mimic (50 nM) caused a significant decrease in ErbB4 protein expression as detected with a specific ErbB4 antibody. The blot was reprobed for calnexin to confirm equal loading. A significant decrease in ErbB4/calnexin ratio (40.5% decrease compared to negative control miRNA) was seen in cells transfected with a mir-193b-3p mimic in triplicate wells. Data was from 3 separate experiments.

Fig 4. The expression and activation of two ErbB4 isoforms is increased in ADPKD cystic cells and kidney tissue

(A) Expression of full-length uncleaved ErbB4 (180 kDa) was increased in ADPKD cells compared to controls. Blots were reprobed for calnexin to confirm equal loading. The ErbB4/calnexin ratio in ADPKD cells was significantly increased compared to controls. Data is presented as an average of 3 separate repeat experiments. **(B).** Schematic diagram of ErbB4 depicting the position of primers used to amplify domains present in different isoforms. **(C)** Isoform specific primers were designed to amplify endogenous JM-a, CYT-1/2 or all ErbB4 from OX161 mRNA by RT-PCR. A plasmid expressing the JM-a CYT-1 isoform of ErbB4 (pcDNA3.1-ErbB4) was used as a positive control template. Two isoforms, JM-a CYT-1 and JM-a CYT-2, were found to be present in OX161. **(D)** The two ErbB4 isoforms JM-a CYT-1 and JM-a CYT-2 were similarly expressed in all normal and ADPKD cell lines tested. **(E)** Increased expression of ErbB4 was observed in cyst lining epithelial cells of kidney tissue sections from patients with ADPKD (n=7) compared to controls (n=3). Nuclear localisation of ErbB4 was detected in ErbB4 positive cysts (black arrows) indicating ErbB4 cleavage and activation of gene transcription. **(F)** Nuclear ErbB4 expression was significantly increased in ErbB4 positive cysts in ADPKD kidneys compared to controls.. *** P<0.001. **(G)** ErbB4 mRNA was significantly increased in kidneys derived from *Cre;Pkd1*$^{del2–11,lox}$ mice at 4 months after Tamoxifen compared to untreated control animals (n=4-5) as detected by Taqman qPCR assays. **(H)** Increased expression of ErbB4 was seen in the cyst lining epithelial cells of cystic kidneys from *Cre;Pkd1*$^{del2–11,lox}$ mice 3 and 4 month after tamoxifen induction compared to control un-induced animals (n=6 each). Nuclear localisation of ErbB4 was observed in ErbB4 positive cysts (black arrows) indicating ErbB4 cleavage and activation of gene transcription. **(I)** Nuclear ErbB4 expression was significantly increased in ErbB4 positive cysts in *Cre;Pkd1*$^{del2–11,lox}$ mice compared to control mice 2, 3 and 4 month after treatment with tamoxifen *** P<0.001. **(J)** mir193b-3p miRNA was significantly decreased in kidneys derived from *Cre;Pkd1*$^{del2-11,lox}$ mice at 4 months after Tamoxifen compared to untreated control animals (n=4-5) as detected by Taqman qPCR.

Fig 5. Increased ErbB4 in urinary extracellular vesicles from ADPKD patients correlates with renal disease progression.

(A) Electron microscopy of purified urinary extracellular vesicles. Extracellular vesicles with a diameter <100nm can be seen (arrows) indicating successful purification of urinary exosomes (magnification x 26000). An expanded view of a cluster of vesicles (box in A) shows a measured diameter of 66.7nm in a typical vesicle. **(B)** Immunoblotting of cell free urine, exosome preparation supernatant, concentrated cell free urine and exosome pellet. Expression of TSG-101 was observed only in the exosome pellet fraction, indicating purification of urinary exosomes. Tamm-Horsfall protein (THP) and Aquaporin-2 (AQP2) were present in concentrated cell free urine as well as in the exosome pellet. **(C)** Representative blot showing increased ErbB4 expression in ADPKD patient urine exosomes compared to normal controls (n=12). The arrowhead indicates an 80 kDa ErbB4 C-terminal cleavage product; the asterisk indicates a possible non-specific band around 50kDa. The exosome specific protein TSG-101 was used as a loading control. **(D)** A significant increase in ErbB4 expression was seen in ADPKD patient urine exosomes with an eGFR<60 (n=16) compared to controls (n=12) or ADPKD patients with an eGFR>60 (n=16). ***p<0.001, ****p<0.0001. **(E)** ROC curves for exosome associated ErbB4 for dichotomized GFR slope (cut-off > or < -3 ml/min). ErbB4 had a higher AUC than mean kidney length reflecting the ability to discriminate between patients with higher risk of progression. The AUC was significantly increased (p=0.002) when ErBB4 was combined with mean kidney length.

Fig 6. Activation of ErbB4 dependent cell proliferation, signalling and cytogenesis is increased in ADPKD cells.

(A) Addition of the ErbB4 ligand NRG-1 (100 ng/ml) resulted in a significantly greater increase in proliferation from baseline in ADPKD compared to control cells by a BrdU incorporation assay. ** $p<0.01$, *$p<0.05$. **(B)** NRG-1 incubation led to a much higher level of phosphorylated ErbB4 (pErbB4) in ADPKD compared to normal controls. pErbB4 (Tyr1118) was detected as two bands (arrowheads) representing full-length (180kDa) and C-terminal cleaved (80kDa) proteins. The blot was reprobed for actin to check for loading. The pErbB4/actin ratio in ADPKD cells was significantly higher compared to controls. Data is presented as an average of 3 separate repeat experiments (graph in lower panel). **(C)** ADPKD **(**OX161) cells stimulated with NRG-1 (1-100 ng/ml) for 15 min show a greater increase in pERK and pAKT compared to Normal (N, UCL93) cells. Basal pAKT was also noticeably higher in unstimulated ADPKD cells. Equal loading was confirmed by reprobing for total ERK or AKT. Representative blot of three experiments. The pAKT/total AKT and pERK/total ERK ratio in ADPKD cells were significantly higher following stimulation with 10 and 100ng/ml NRG-1 compared to controls. Data is presented as an average of 3 separate repeat experiments (graphs). **(D)** HB-EGF incubation (100ng/ml for 15 min) led to an increase in phosphorylated ErbB4 (pErbB4) in ADPKD cells. pErbB4 (Tyr1118) was detected as two bands representing full-length (180kDa) and C-terminal cleaved (80kDa) proteins. The blot was reprobed for actin to check for loading. **(E)** OX161 cells form cysts with visible lumen in a time dependent manner when cultured in a 3D matrix (matrigel) over 12 days. **(F)** There was a significant increase in average cyst area in cells cultured with 100 ng/ml NRG-1 or HB-EGF compared to untreated cells. **** $p<0.0001$ by 2 way ANOVA.

Fig 7. ErbB4 mediates proliferation in ADPKD cell lines.

(A) Transfection of control cells (UCL93) with pcDNA3.1-ErbB4 plasmid was associated with a significant increase in cell proliferation as measured by BrDU incorporation, compared to untransfected cells or cells transfected with a pcDNA3.1 empty vector.****p<0.0001. (**B)** Transfection of ADPKD cells (OX161) with specific ErbB4 siRNA resulted in a significant reduction in ErbB4 mRNA detected by Taqman qPCR assay representing a fold change of 0.4036 relative to scrambled control siRNA. **(C)** Transfection of OX161 cells with specific ErbB4 siRNA resulted in a significant reduction in proliferation compared to cells transfected with a negative, scrambled control siRNA.*p<0.05**.** The fold change reduction in ErbB4 mRNA by ErbB4 specific siRNA was detected by Taqman qPCR assay and showed a fold change of 0.4036 relative to scrambled control siRNA**. (D)** Incubation of cells with a pan-ErbB small molecule inhibitor (JNJ 28871063) for 24 h resulted in a dose-dependent decrease in cell proliferation in ADPKD (OX161) cells compared to controls. *p<0.05, **p<0.01. **(E)** Incubation of cells with an ErbB4 specific blocking antibody (H4.72.8) for 24 h led to a significant reduction in cell proliferation in ADPKD (OX161) cells compared to controls. *p<0.05, **p<0.01, ***p<0.001. **(F)** A non-specific control mouse IgG for 24 h had no effect on cell proliferation in ADPKD (OX161) cells compared to controls.

Fig 1

A.

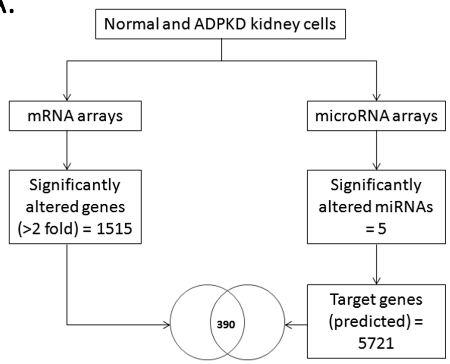

B.

Analysis Type: PANTHER Overrepresentation Test (release 20150430)		
Annotation Version and Release Date: PANTHER version 10.0 Released 2015-05-15		
Reference List: Homo sapiens (all genes in database)		
Analyzed List: Up-regulated genes > 2 fold		
PANTHER Pathways	**Fold Enrichment**	**P-value**
FGF signaling pathway (P00021)	4.17	1.67E-03
Gonadotropin releasing hormone receptor pathway (P06664)	2.93	4.17E-03
Alpha adrenergic receptor signaling pathway (P00002)	> 5	5.09E-03
Histamine H1 receptor mediated signaling pathway (P04385)	> 5	7.64E-03
EGF receptor signaling pathway (P00018)	3.38	9.46E-03
MYO_signaling_pathway (P06215)	> 5	1.36E-02
GBB_signaling_pathway (P06214)	> 5	1.36E-02
Activinbetasignaling_pathway (P06210)	> 5	1.36E-02
ALP23B_signaling_pathway (P06209)	> 5	1.36E-02
Angiogenesis (P00005)	2.86	2.01E-02
Apoptosis signaling pathway (P00006)	3.19	2.17E-02
Oxytocin receptor mediated signaling pathway (P04391)	5	2.30E-02
Thyrotropin-releasing hormone receptor signaling pathway (P04394)	4.78	2.58E-02
SCW_signaling_pathway (P06216)	> 5	2.69E-02
DPP_signaling_pathway (P06213)	> 5	2.69E-02
DPP-SCW_signaling_pathway (P06212)	> 5	2.69E-02
BMP_signaling_pathway-drosophila (P06211)	> 5	2.69E-02
Wnt signaling pathway (P00057)	2.13	2.75E-02
CCKR signaling map (P06959)	2.6	2.97E-02
5HT2 type receptor mediated signaling pathway (P04374)	4.31	3.34E-02
Thiamine metabolism (P02780)	> 5	4.01E-02
Toll receptor signaling pathway (P00054)	3.93	4.22E-02
Analyzed List: Down-regulated genes > 2 fold		
PANTHER Pathways	**Fold Enrichment**	**P-value**
Heterotrimeric G-protein signaling pathway-Gi alpha and Gs alpha mediated pathway (P00026)	2	9.84E-03
Heterotrimeric G-protein signaling pathway-Gq alpha and Go alpha mediated pathway (P00027)	2.11	1.07E-02
Ionotropic glutamate receptor pathway (P00037)	2.57	1.44E-02
Enkephalin release (P05913)	3.66	2.51E-02
Cadherin signaling pathway (P00012)	1.72	2.76E-02
Nicotine pharmacodynamics pathway (P06587)	2.77	3.65E-02
Metabotropic glutamate receptor group II pathway (P00040)	2.69	4.06E-02
Heterotrimeric G-protein signaling pathway-rod outer segment phototransduction (P00028)	2.69	4.06E-02

Fig 2

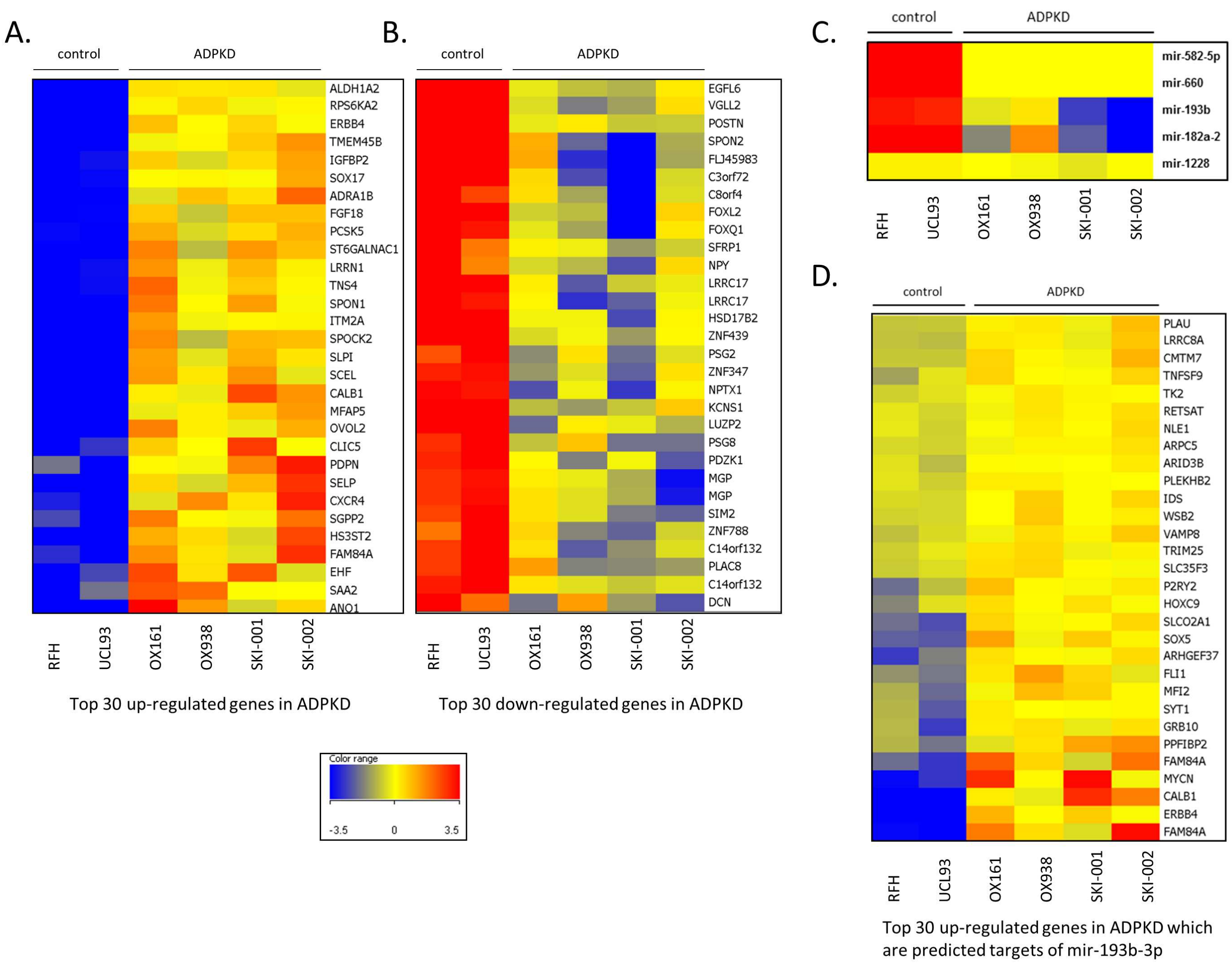

A.
control
ADPKD
ALDH1A2
RPS6KA2
ERBB4
TMEM45B
IGFBP2
SOX17
ADRA1B
FGF18
PCSK5
ST6GALNAC1
LRRN1
TNS4
SPON1
ITM2A
SPOCK2
SLPI
SCEL
CALB1
MFAP5
OVOL2
CLIC5
PDPN
SELP
CXCR4
SGPP2
HS3ST2
FAM84A
EHF
SAA2
ANO1
RFH
UCL93
OX161
OX938
SKI-001
SKI-002
Top 30 up-regulated genes in ADPKD
B.
control
ADPKD
EGFL6
VGLL2
POSTN
SPON2
FLJ45983
C3orf72
C8orf4
FOXL2
FOXQ1
SFRP1
NPY
LRRC17
LRRC17
HSD17B2
ZNF439
PSG2
ZNF347
NPTX1
KCNS1
LUZP2
PSG8
PDZK1
MGP
MGP
SIM2
ZNF788
C14orf132
PLAC8
C14orf132
DCN
RFH
UCL93
OX161
OX938
SKI-001
SKI-002
Top 30 down-regulated genes in ADPKD
Color range
-3.5
0
3.5
C.
control
ADPKD
mir-582-5p
mir-660
mir-193b
mir-182a-2
mir-1228
RFH
UCL93
OX161
OX938
SKI-001
SKI-002
D.
control
ADPKD
PLAU
LRRC8A
CMTM7
TNFSF9
TK2
RETSAT
NLE1
ARPC5
ARID3B
PLEKHB2
IDS
WSB2
VAMP8
TRIM25
SLC35F3
P2RY2
HOXC9
SLCO2A1
SOX5
ARHGEF37
FLI1
MFI2
SYT1
GRB10
PPFIBP2
FAM84A
MYCN
CALB1
ERBB4
FAM84A
RFH
UCL93
OX161
OX938
SKI-001
SKI-002
Top 30 up-regulated genes in ADPKD which are predicted targets of mir-193b-3p

Fig 3

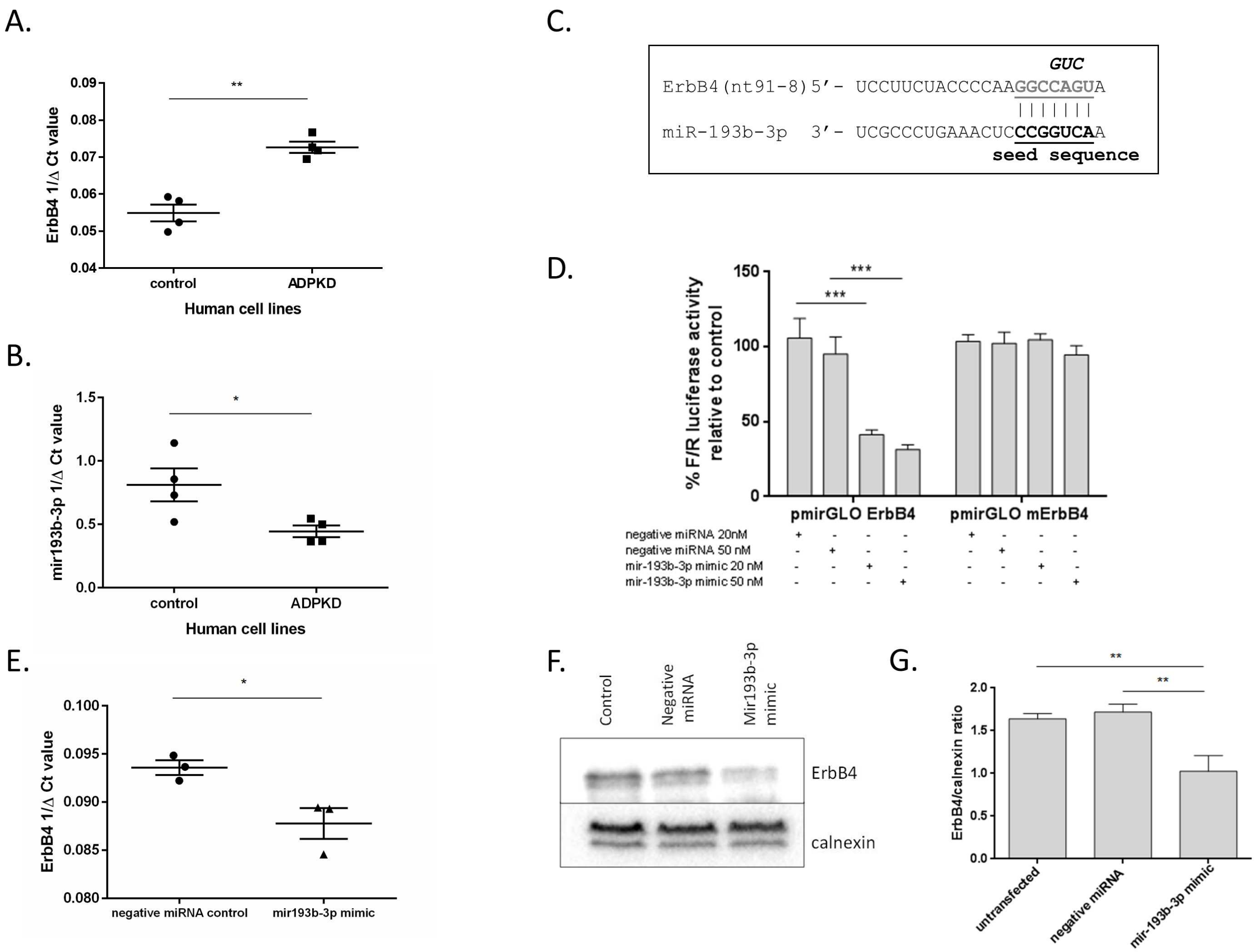

A.
ErbB4 1/Δ Ct value
0.09
0.08
0.07
0.06
0.05
0.04
**
control
ADPKD
Human cell lines
B.
mir193b-3p 1/Δ Ct value
1.5
1.0
0.5
0.0
*
control
ADPKD
Human cell lines
C.
GUC
ErbB4(nt91-8)5'- UCCUUCUACCCCAAGGCCAGUA
miR-193b-3p 3'- UCGCCCUGAAACUCCCGGUCAA
seed sequence
D.
% F/R luciferase activity relative to control
150
100
50
0
***
***
pmirGLO ErbB4
pmirGLO mErbB4
negative miRNA 20nM
negative miRNA 50 nM
mir-193b-3p mimic 20 nM
mir-193b-3p mimic 50 nM
E.
ErbB4 1/Δ Ct value
0.100
0.095
0.090
0.085
0.080
*
negative miRNA control
mir193b-3p mimic
F.
Control
Negative miRNA
Mir193b-3p mimic
ErbB4
calnexin
G.
ErbB4/calnexin ratio
2.0
1.5
1.0
0.5
0.0
**
**
untransfected
negative miRNA
mir-193b-3p mimic

Fig 4

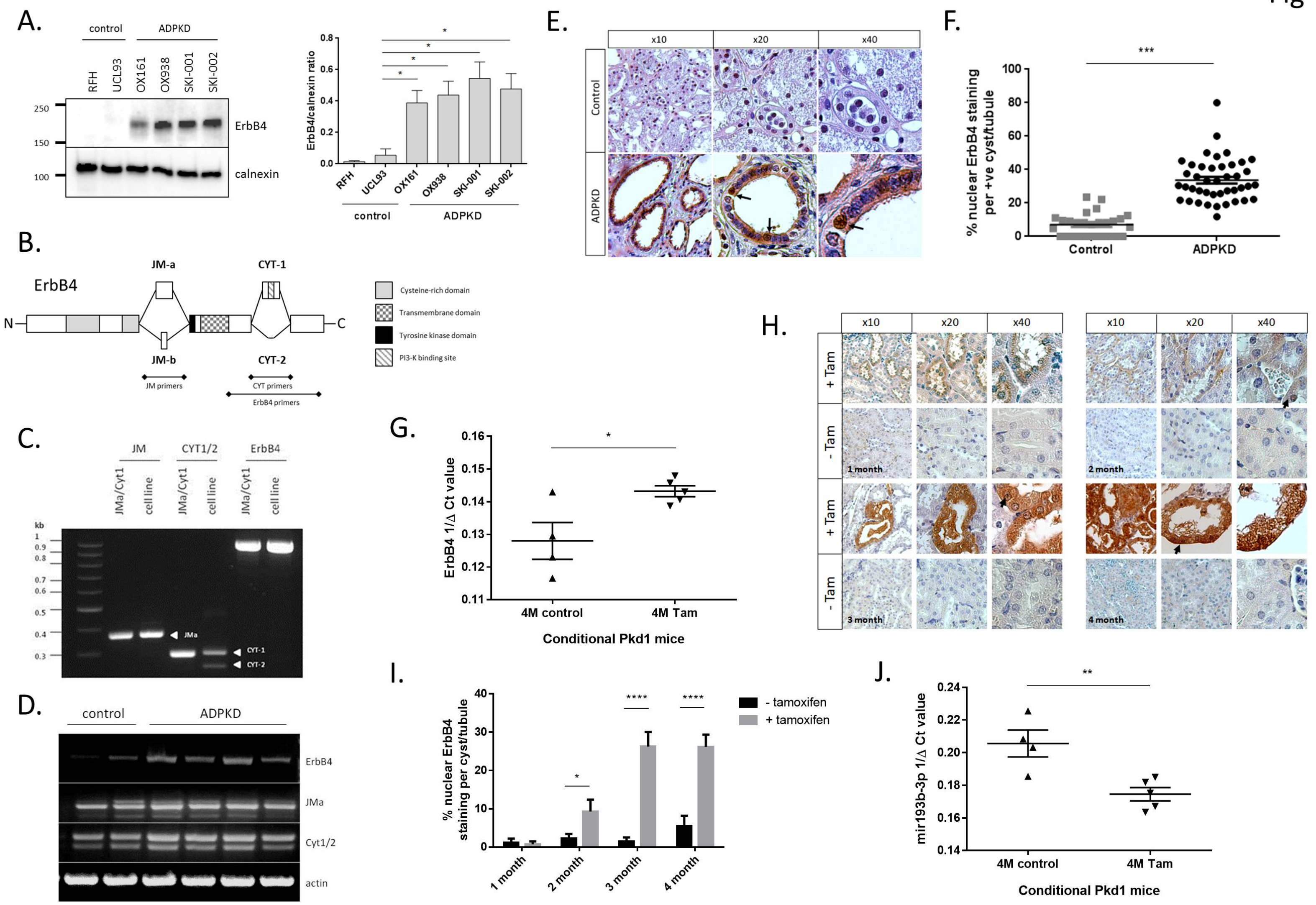
A.
control
ADPKD
RFH
UCL93
OX161
OX938
SKI-001
SKI-002
250
150
100
ErbB4
calnexin
ErbB4/calnexin ratio
control
ADPKD
B.
ErbB4
JM-a
JM-b
CYT-1
CYT-2
N
C
JM primers
CYT primers
ErbB4 primers
Cysteine-rich domain
Transmembrane domain
Tyrosine kinase domain
PI3-K binding site
C.
JM
CYT1/2
ErbB4
JMa/Cyt1
cell line
kb
JMa
CYT-1
CYT-2
D.
control
ADPKD
ErbB4
JMa
Cyt1/2
actin
E.
x10
x20
x40
Control
ADPKD
F.
% nuclear ErbB4 staining per +ve cyst/tubule
Control
ADPKD
G.
ErbB4 1/Δ Ct value
4M control
4M Tam
Conditional Pkd1 mice
H.
x10
x20
x40
+ Tam
- Tam
1 month
2 month
3 month
4 month
I.
% nuclear ErbB4 staining per cyst/tubule
- tamoxifen
+ tamoxifen
1 month
2 month
3 month
4 month
J.
mir193b-3p 1/Δ Ct value
4M control
4M Tam
Conditional Pkd1 mice

Fig 5

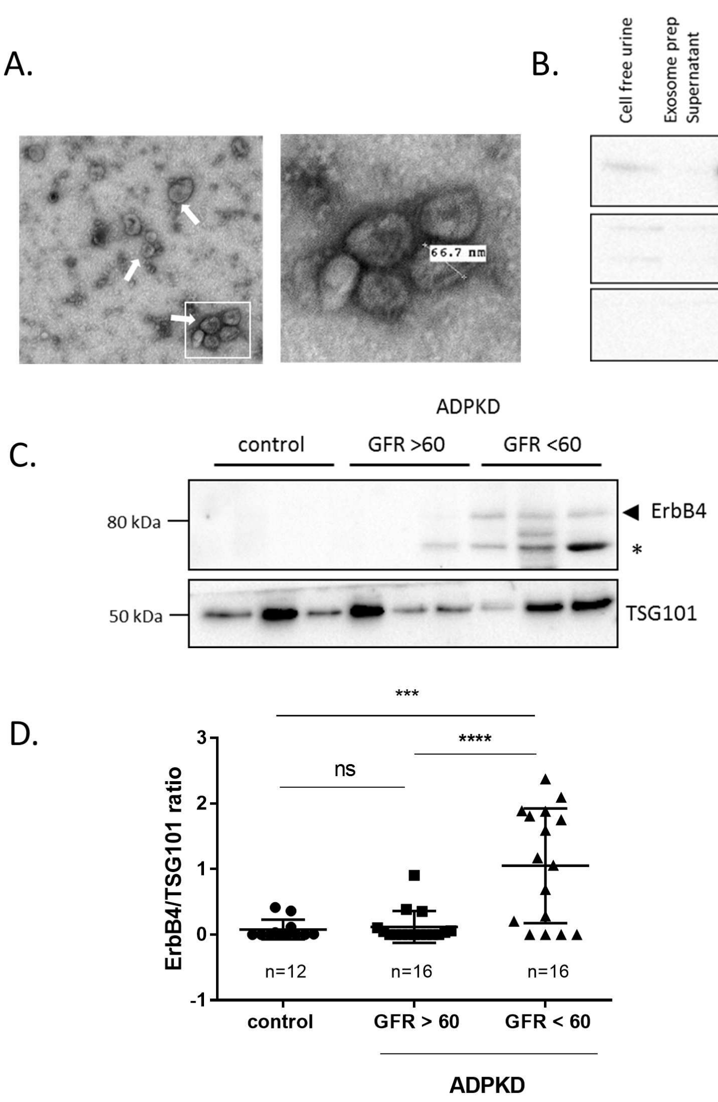

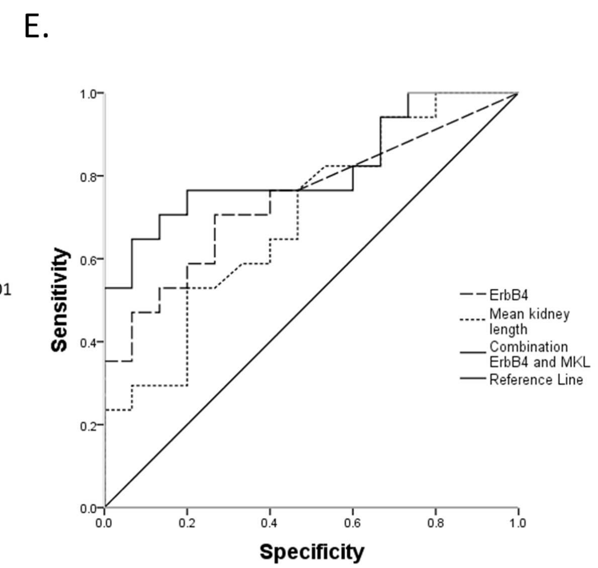

Variables	AUC	95 % CI	P value
ErbB4	0.745	0.573-0.917	0.018
Mean kidney length	0.698	0.516-0.880	0.057
ErbB4 and MKL	0.816	0.665-0.967	0.002

Fig 6

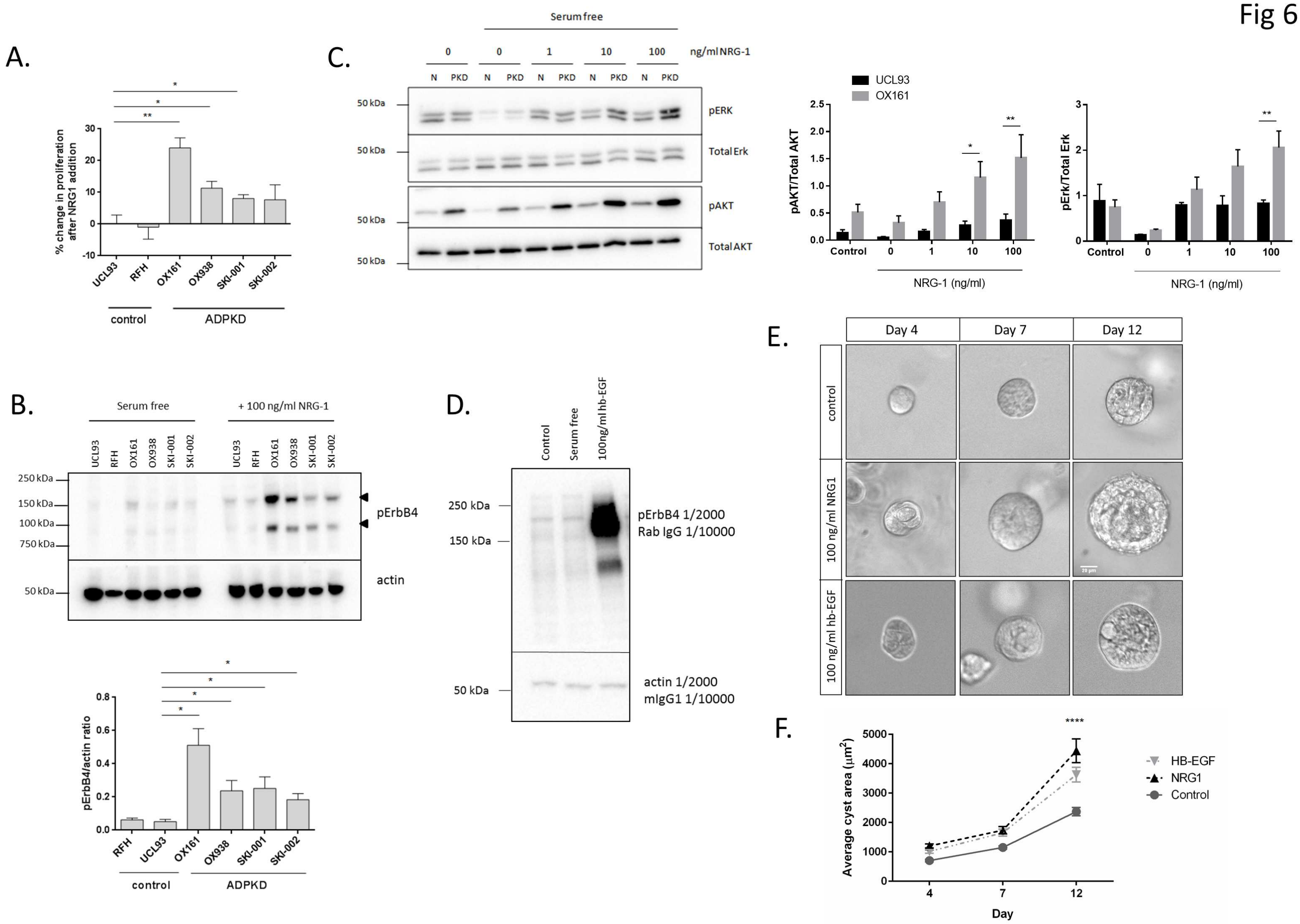

A.
% change in proliferation after NRG1 addition
UCL93
RFH
OX161
OX938
SKI-001
SKI-002
control
ADPKD
B.
Serum free
+ 100 ng/ml NRG-1
pErbB4
actin
pErbB4/actin ratio
C.
Serum free
ng/ml NRG-1
pERK
Total Erk
pAKT
Total AKT
UCL93
OX161
pAKT/Total AKT
pErk/Total Erk
Control
NRG-1 (ng/ml)
D.
Control
Serum free
100ng/ml hb-EGF
pErbB4 1/2000
Rab IgG 1/10000
actin 1/2000
mIgG1 1/10000
E.
Day 4
Day 7
Day 12
control
100 ng/ml NRG1
100 ng/ml hb-EGF
F.
Average cyst area (μm2)
Day
HB-EGF
NRG1
Control

Fig 7

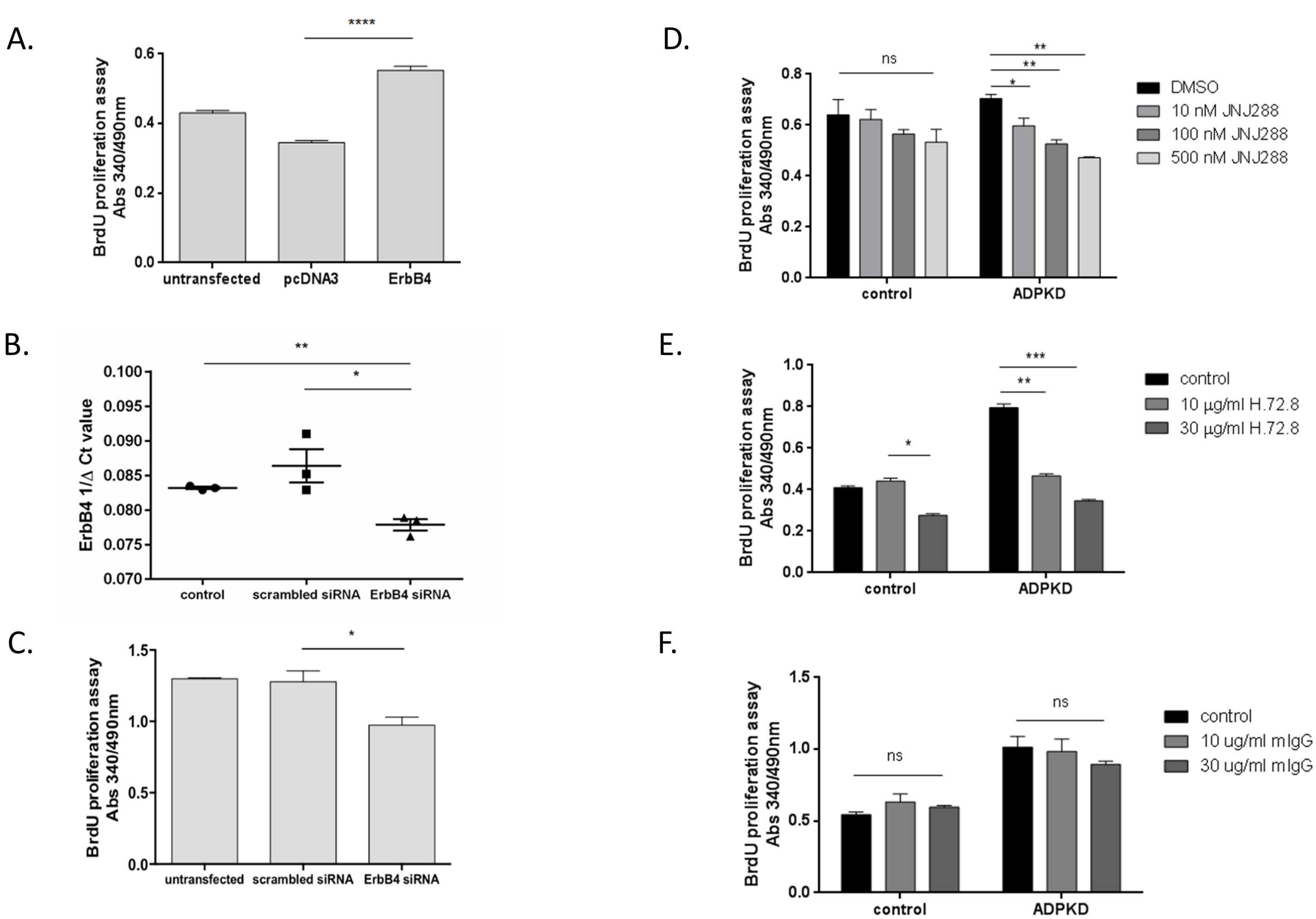
A.
BrdU proliferation assay
Abs 340/490nm
****
0.0
0.2
0.4
0.6
untransfected
pcDNA3
ErbB4
B.
ErbB4 1/Δ Ct value
**
*
0.070
0.075
0.080
0.085
0.090
0.095
0.100
control
scrambled siRNA
ErbB4 siRNA
C.
BrdU proliferation assay
Abs 340/490nm
*
0.0
0.5
1.0
1.5
untransfected
scrambled siRNA
ErbB4 siRNA
D.
BrdU proliferation assay
Abs 340/490nm
ns
**
**
*
0.0
0.2
0.4
0.6
0.8
control
ADPKD
DMSO
10 nM JNJ288
100 nM JNJ288
500 nM JNJ288
E.
BrdU proliferation assay
Abs 340/490nm
***
**
*
0.0
0.2
0.4
0.6
0.8
1.0
control
ADPKD
control
10 µg/ml H.72.8
30 µg/ml H.72.8
F.
BrdU proliferation assay
Abs 340/490nm
ns
ns
0.0
0.5
1.0
1.5
control
ADPKD
control
10 ug/ml mIgG
30 ug/ml mIgG